

UCSF

UC San Francisco Previously Published Works

Title

Flow stimuli reveal ecologically appropriate responses in mouse visual cortex

Permalink

<https://escholarship.org/uc/item/6m50k1jt>

Journal

Proceedings of the National Academy of Sciences of the United States of America, 115(44)

ISSN

0027-8424

Authors

Dyballa, Luciano
Hoseini, Mahmood S
Dadarlat, Maria C
et al.

Publication Date

2018-10-30

DOI

10.1073/pnas.1811265115

Peer reviewed



Flow stimuli reveal ecologically appropriate responses in mouse visual cortex

Luciano Dyballa^{a,1}, Mahmood S. Hoseini^{b,1}, Maria C. Dadarlat^b, Steven W. Zucker^{a,c}, and Michael P. Stryker^{b,2}

^aDepartment of Computer Science, Yale University, New Haven, CT 06520; ^bCenter for Integrative Neuroscience, University of California, San Francisco, CA 94143-0444; and ^cDepartment of Biomedical Engineering, Yale University, New Haven, CT 06520

Contributed by Michael P. Stryker, September 4, 2018 (sent for review July 5, 2018; reviewed by Lindsey L. Glickfeld and Christopher M. Niell)

Assessments of the mouse visual system based on spatial-frequency analysis imply that its visual capacity is low, with few neurons responding to spatial frequencies greater than 0.5 cycles per degree. However, visually mediated behaviors, such as prey capture, suggest that the mouse visual system is more precise. We introduce a stimulus class—visual flow patterns—that is more like what the mouse would encounter in the natural world than are sine-wave gratings but is more tractable for analysis than are natural images. We used 128-site silicon microelectrodes to measure the simultaneous responses of single neurons in the primary visual cortex (V1) of alert mice. While holding temporal-frequency content fixed, we explored a class of drifting patterns of black or white dots that have energy only at higher spatial frequencies. These flow stimuli evoke strong visually mediated responses well beyond those predicted by spatial-frequency analysis. Flow responses predominate in higher spatial-frequency ranges (0.15–1.6 cycles per degree), many are orientation or direction selective, and flow responses of many neurons depend strongly on sign of contrast. Many cells exhibit distributed responses across our stimulus ensemble. Together, these results challenge conventional linear approaches to visual processing and expand our understanding of the mouse's visual capacity to behaviorally relevant ranges.

visual cortex | flow movie | mouse | spatial frequency | receptive field

The mouse has become a major model for studying vision because of the genetic, imaging, and molecular tools available (1). Studies have revealed relationships between macroscopic states of the brain and activity in visual cortex [running vs. stationary (2, 3), pupil size and activity (4, 5), and visual interest (e.g., refs. 5–7)]. However, a basic conundrum has arisen: Behaviorally, mice are capable of sharp, visually mediated behaviors (8–10), such as accurate prey capture (11), but when assessed using standard assays, such as spatial-frequency gratings (Fig. 1), the mouse appears to have very poor vision. Although orientation selectivity has been found (12), receptive fields are large [typically $\geq 25^\circ$] when estimated by spike-triggered averaging, and spatial-frequency tuning is concentrated below 0.08 cycles per degree (cpd). While this motivates the use of gratings at 0.04 cpd in experiments, it raises the question, How does the visual system perform so exquisitely in natural tasks?

We show here that ecologically relevant stimuli can exercise mouse visual cortex in manifold ways. While plaids (13, 14) and random-dot kinematograms (15, 16) are a step beyond gratings, the leap to natural images (e.g., ref. 17) is more common (e.g., refs. 18 and 19). However, natural images are difficult to obtain (20), difficult to control parametrically, and difficult to analyze beyond second order (21).

For a mouse running through a field, the visual display is like a “waterfall” of illuminated material flowing past, with bright- or dark-oriented segments arising from complex photometric events (Fig. 1A) (22). This visual metaphor motivates our stimuli. We approximate such patterns with a class of visual flows composed of dots. These are more natural than drifting grat-

ings but can be parametrically controlled in their orientation (content and angle), spatial frequency, and direction of motion. We call them flows because, intuitively, they consist of a field of particles (either dots or dotted-line segments) dropped into a “flowing river.” More formally, each dot is displaced along a vector field in space and time and follows a dynamical system (23). When the orientation structure is removed, the flows reduce to random-dot kinematograms; when the temporal structure is removed, the flows reduce to static Glass patterns (24). Thus, they are rich in geometry and, for humans, the perception of such flows differs from strictly aligned patterns (25, 26). Parametric variations in orientation, direction, etc., define an ensemble of stimuli.

We here explore activity in mouse primary visual cortex (V1) in response to the flow ensemble. In many cases flow stimuli elicit more vigorous responses than drifting gratings, particularly at high spatial frequencies 3–5 octaves above 0.04 cpd. Some V1 neurons are classical, resembling feature detectors, while others exhibit a mixed selectivity rarely reported in early visual cortex. The rich ensemble of selectivities in V1 may equip the mouse to behave in the natural world.

Results

Cells in V1 Have Diverse Preferred Stimuli. We developed an ensemble of stimuli including drifting gratings, single-dot flows (random-dot kinematograms), and oriented flows where each element consists of three or four dots (*Materials and Methods*). The stimuli had either positive contrast (bright dots) or negative

Significance

The visual system of the mouse is now widely studied as a model for development and disease in humans. Studies of its primary visual cortex (V1) using conventional grating stimuli to construct linear–nonlinear receptive fields suggest that the mouse must have very poor vision. Using stimuli resembling the flow of images across the retina as the mouse moves through the grass, we find that most V1 neurons respond reliably to very much finer details of the visual scene than previously believed. Our findings suggest that the conventional notion of a unique receptive field does not capture the operation of the neural network in mouse V1.

Author contributions: L.D., M.S.H., S.W.Z., and M.P.S. designed research; M.S.H. and M.C.D. performed research; L.D. and S.W.Z. analyzed data; L.D., M.S.H., S.W.Z., and M.P.S. wrote the paper; L.D. designed and implemented stimuli; and S.W.Z. designed the stimuli.

Reviewers: L.L.G., Duke University; and C.M.N., University of Oregon.

The authors declare no conflict of interest.

Published under the PNAS license.

Data deposition: Computer code used to generate stimuli has been deposited at <https://github.com/zuckerlab/FlowStims>.

¹L.D. and M.S.H. contributed equally to this work.

²To whom correspondence should be addressed. Email: stryker@phy.ucsf.edu.

This article contains supporting information online at www.pnas.org/lookup/suppl/doi:10.1073/pnas.1811265115/-DCSupplemental.

Published online October 16, 2018.

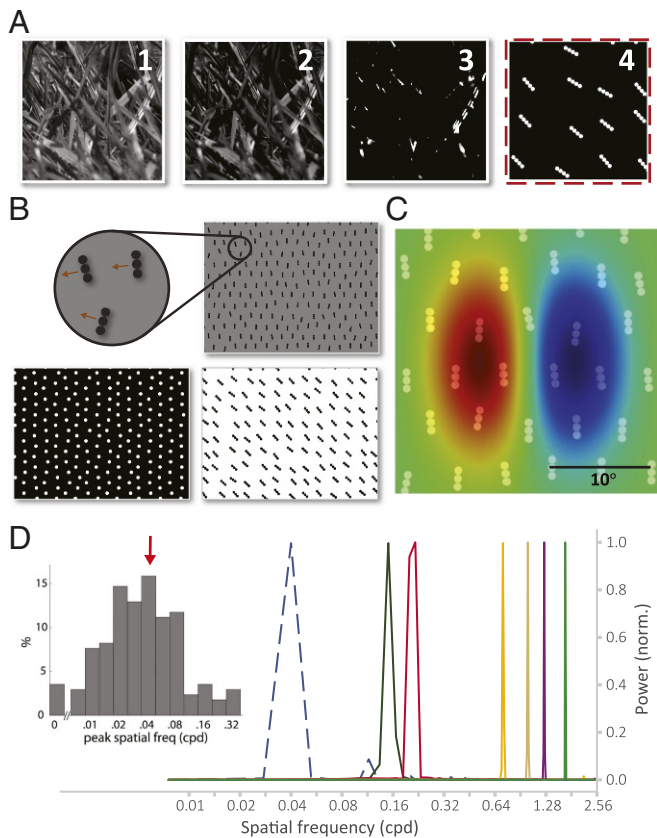


Fig. 1. Introducing flow stimuli. (A) Ecological motivation. Working with a single frame (A, 1–3), a grassy patch is modified to emphasize salient higher contrasts. Our abstraction (the flow field in A, 4) approximates this with a binary pattern of random, oriented dotted segments. (B) We generalize to flow fields consisting of dotted segments of different lengths, emphasizing two geometries [oriented (three or four aligned dots) or nonoriented (single dots)], two contrast polarities (positive or negative), different contrast magnitudes, and various sizes. The full flow stimulus is a movie of one such flow field, drifting across the screen with small random perturbations to suppress rigidity (*Materials and Methods*) (examples in *SI Appendix, Movies S1 and S2*). (C) Flow responses are inconsistent with classical filtering views of V1. Shown is a Gabor receptive field at 0.04 cpd superimposed onto the three-dot flow whose energy peaks at 0.24 cpd (example in B, *Top Right*), for comparison. (D) The 1D discrete Fourier transforms (single sided) of the flows used in our experiments (peaks at 0.15 cpd, 0.24 cpd, 0.7 cpd, 1.0 cpd, 1.25 cpd, and 1.6 cpd) have power well beyond 0.04 cpd (dashed curve), which is the spatial frequency previously reported as optimal for cells in mouse V1 (compare D, *Inset*). Adapted with permission from ref. 12. To compare stimuli, each spectrum is normalized by the power at the peak frequency (norm) (2D spectra in *SI Appendix, Figs. S14 and S15*).

contrast (dark dots). Activity is plotted as an array of peristimulus time histograms (PSTHs) and tuning curves for each unit, to facilitate a quick assessment of the different “dimensions” of a cell’s response. Experiments were conducted in two cohorts, the first one with grating stimuli at 0.04 cpd and both grating and flow stimuli at 0.15 cpd and 0.24 cpd and the second cohort with grating stimuli at 0.04 cpd and both grating and flow stimuli at 0.7 cpd, 1.0 cpd, 1.25 cpd, and 1.6 cpd. All stimuli in both cohorts had a fixed temporal frequency of 4 Hz.

We begin with example cells from cohort 1. The first one (Fig. 2A) has the response profile one would expect for a simple cell in V1. It responds almost exclusively to low-frequency gratings; the PSTHs for high-frequency gratings and for flows (both one-dot and three-dot elements) remain virtually at baseline. Its spike-triggered average (STA) depicts a classical receptive field, consistent with the frequency response, and it is well tuned for

orientation. But such cells were relatively rare in our experiments (discussed below). Another example (Fig. 2B) exhibits a weak response to gratings and a stronger response to flows. The STA, which would predict a strong response to low-frequency gratings, completely fails to predict this response profile. Finally, many cells are multidimensional (Fig. 2C): They respond well to several stimuli from the ensemble, including gratings and flows at multiple spatial frequencies. Note the diversity in the temporal response profile: a periodic (often interpreted as linear) response to gratings at low spatial frequency; a sustained (interpreted as nonlinear) response to gratings at higher frequencies; and a transient burst of activity to positive, oriented flows. It would be inappropriate to label this cell a classical feature detector. The STA again does not predict the response profile, and the PSTHs reveal different tuning widths and different first-spike latencies, as well as linear vs. nonlinear and transient vs. sustained responses.

Responses to Optimal Flows Span a Wide Range of Spatial Frequencies. To quantify this diversity at the population level, we relaxed the notion of a unique preferred stimulus for a cell to allow for multiple possible preferences, according to the following definitions. While this leads to a crude classification of cell types, we stress that it is merely a set of labels for discussion; the underlying complexity remains in the PSTHs.

An individual stimulus is significant for a particular cell if the average firing rate for that stimulus is significantly higher than that for its preceding interstimulus interval (Mann–Whitney *U* test). A cell prefers a stimulus class (e.g., flows or gratings) if at least one variation of that class (spatial frequency, geometry, or contrast polarity) is significant and has average peak firing rate significantly higher than the peak firing rates of all significant variations of the other class (Kruskal–Wallis rank-sum test, Conover–Iman post hoc, Bonferroni correction, $P < 0.05$). When there is no preferred stimulus class but there are significant stimuli in both classes, we classify the cell as multiclass, or simply *multi*. Thus, the preferred stimulus class, or type of a cell, is one of *grating*, *flow*, *multi*, *nonselective*. By this classification, the cell in Fig. 2A would be classified as a *grating* cell, Fig. 2B would be a *flow* cell, and Fig. 2C would be a *multi* cell.

Once each cell’s type, or preferred stimulus class, has been determined, its preferred spatial frequency can be defined as the one with highest average firing rate among all significant variations of the preferred class (or classes, when cells are labeled *multi*).

We plot the proportion of preferred types at each preferred frequency in Fig. 2D; the two separate plots denote units from experimental cohort 1 (0.04–0.24 cpd, $n = 357$ cells, three animals) and cohort 2 (0.04–1.6 cpd, $n = 256$ cells, three animals), respectively. Note the predominance of *gratings* among cells at the lowest frequency, replicating Fig. 1D, *Inset*, and the predominance of *flow* and *multi* types at the higher frequencies.

We now examine the distribution of preferred types in two different ways, either including or not including the responses to low-frequency gratings. This is necessary, since the performance measure is a simple spike statistic that is easily dominated by the gratings. First, when low-frequency gratings are included among the stimuli, by the above definitions 45% of the cells respond equally well (i.e., are of the *multi* type), 28% are *flow* cells, 26% prefer *gratings*, and 29% of the cells were not significantly responsive to any of the stimuli displayed (Fig. 2E, blue). When low-frequency gratings are not included, so that the comparison is among flows and gratings at the same spatial frequencies, responses favoring *flow* (50%) and *multi* (43%) predominate over those favoring *gratings* (7%) (Fig. 2E, red). The difference between these two plots comes from a more detailed analysis: The cells responding strongly to 0.04 cpd can be divided into roughly two subgroups: one that has no significant response other

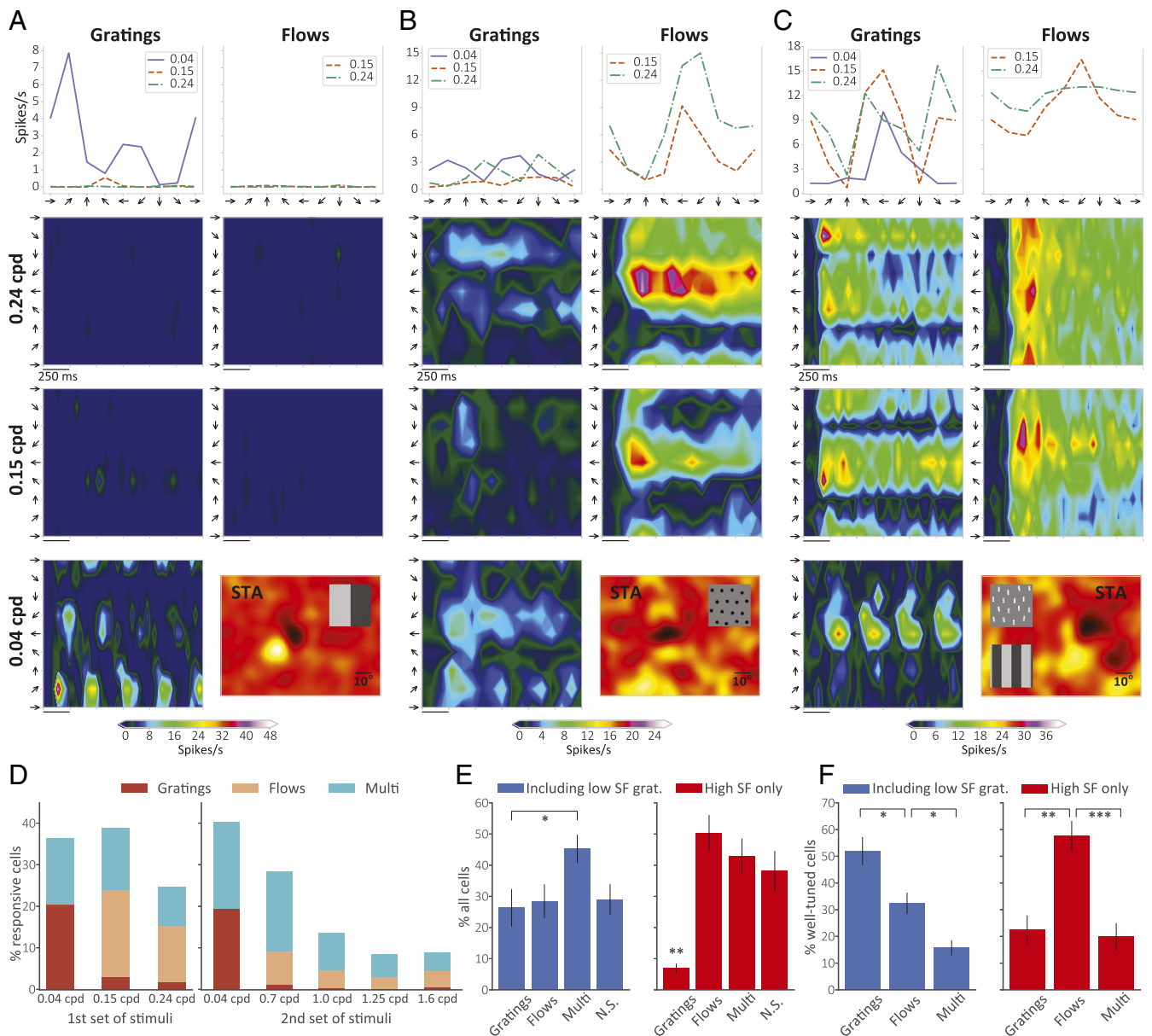


Fig. 2. Variety of responses in V1. (A–C) Tuning curves and PSTHs of three example cells in response to drifting gratings and flows at 0.04 cpd, 0.15 cpd, and 0.24 cpd in eight equally spaced directions of motion. Time axis in histograms encompasses an entire period of stimulus presentation (1.5 s). *Insets* in (B) Cell responding preferentially to single-dot flows with negative contrast. Bin size is 83 ms. (C) Cell responding strongly to both oriented (three dots), positive flows and gratings (at both high and low spatial frequencies). Bin size is 46 ms. (D) Distribution of optimal spatial frequency in terms of proportion of cells significantly responding to at least one of the stimuli. In the group of experiments using the first set of stimuli (*D, Left*, 0.04–0.24 cpd, $n = 357$ cells, three animals), the majority of cells fired more strongly for stimuli at 0.15 cpd, followed closely by 0.04 cpd. For the second set of stimuli (*D, Right*, 0.04–1.6 cpd, $n = 256$ cells, three animals) there was an overwhelming preference for 0.04 cpd, although more than half the cells had optimal spatial frequency in the range 0.7–1.6 cpd. (E) Distribution of preferred stimulus among all cells. When low-frequency gratings (0.04 cpd) are included among the stimuli (*E, Left*), the majority of cells respond equally well to both classes (“Multi”), followed by only flows and only gratings; 29% of the cells were not significantly responsive (“N.S.”) to any of the stimuli displayed ($n = 1,026$ cells; 10 experiments, six animals). When we do not include low-frequency gratings (grat), thereby limiting the comparison with flows and gratings with similar spatial frequencies, there is a significant preference for flows only and for both over gratings only. Comparison of *E, Left* and *Right* reveals that $\sim 20\%$ of cells preferred low-frequency gratings. When we recompute stimulus preference considering only stimuli with comparable spatial frequencies, most cells that preferred low-frequency gratings now either prefer none of the high-frequency stimuli or significantly prefer flows over high-frequency gratings, given that the fraction that prefers both remains essentially constant in the two scenarios. $*P < 0.025$; $**P < 0.001$. Error bars represent SEM. (F) Distribution of preferred stimulus among well-tuned cells (i.e., those with OSI > 0.5 or DSI > 0.5), $n = 295$ cells (*Left*) and 241 cells (*Right*); 8 experiments, four animals. Here, note that most of the cells responding to orientation and/or direction will fire more strongly to low-frequency gratings; *F, Right* reveals, however, that the fraction of cells well tuned to flows is just as large. And, similarly to *E*, many of the well-tuned cells preferring 0.04 cpd gratings prefer flows to gratings of comparable spatial frequency. $*P < 0.05$; $**P < 0.001$; $***P < 0.0001$. Error bars represent SEM.

than to low-frequency gratings and another that also responds well to flows (or, in fewer cases, to both flows and high-frequency gratings). These plots include all cells. A similar distinction is

obtained when only cells well tuned to orientation [orientation selectivity index (OSI) > 0.5] or direction [direction selectivity index (DSI) > 0.5] are considered (Fig. 2F).

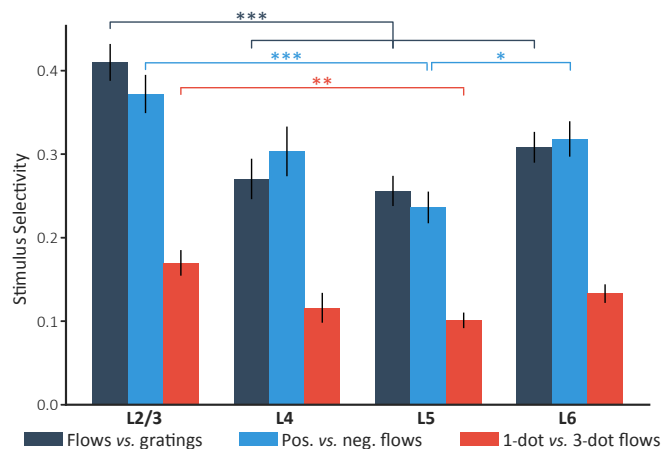


Fig. 4. Cells in different layers have distinct selectivity toward different stimulus classes, as measured by a SSI (main text). *** $P < 0.001$; ** $P < 0.005$; * $P < 0.05$. Error bars represent SEM.

and as “complex” if the response is nonlinear (over phase). However, these are operational definitions and depend on the stimuli. Arguments against such classical receptive field concepts are developing (28), and our results contribute to this. Unlike the traditional, optimal feature viewpoint, selectivity does not appear to be 1D; cells can respond linearly to one part of the stimulus ensemble while being nonlinear to others. In particular, we found many cells that exhibit a “linear” response to low-frequency gratings while also responding vigorously at high spatial frequencies to some type of flow (*SI Appendix, Fig. S16*).

The fact that linear methods (e.g., ref. 29) cannot explain such complex and varied responses to an ensemble of stimuli has several implications (*SI Appendix, Figs. S17 and S18*). First, it brings some of the feature variability seen in higher visual areas (e.g., refs. 30 and 31 and references therein) down to V1. Second, since the receptive field is often taken as the signature of functionality, attempts to relate function to structure based on it (e.g., ref. 32) may attribute to “noise” in connectivity genuine features important for neural responses. It follows that stimulus ensembles richer than low-frequency gratings are required to properly assess visual system function. Finally, it suggests that network computations, not individual features, should be the focus of investigation (33).

Flow Responses Suggest Network Computations. At a small scale, responses to high-frequency flow stimuli (i.e., within a receptive field) are reminiscent of the subzones observed in flies (34) and primates (35), each of which can be direction or orientation selective. And, as in flies (36), many cells with a preference for flow stimuli are also contrast selective. At a large scale, our stimuli were displayed wide field, so extraclassical effects may also be playing a role. While investigations of such contextual interactions in mice are just beginning, when stimuli were restricted to gratings (37) and bars (38), only suppressive effects were observed (39). By contrast, in primates the situation is much richer (40–42), and the arrangements of dots and bars in these studies are reminiscent of our flow stimuli. Despite the fact that mice lack orientation columns (43), flow responses are remarkably consistent among the different species. Flow stimuli are also informative about the geometry of surrounding objects (44), although how these geometric, network computations are realized remains an open question.

Materials and Methods

Animal Procedures. Experiments were performed on adult C57/BL6 mice (age 2–6 mo) of either sex. The animals were maintained in the animal facil-

ity at the University of California, San Francisco and used in accordance with protocols approved by the University of California, San Francisco Institutional Animal Care and Use Committee. Preparation, extracellular recording, and single-neuron analysis were generally performed as in ref. 45. See *SI Appendix, Materials and Methods* for additional materials and methods.

Design of Flow Stimuli. The flow stimuli consist of local flow elements that move according to an underlying displacement field. The displacement field is defined as a vector in \mathbb{R}^2 (i.e., a magnitude and a direction) at each screen position. Each flow element consists of a linear arrangement of n adjacent dots, with $n = 1$ corresponding to a random-dot kinematogram and $n = 2, 3, 4$ corresponding to oriented elements (compare Fig. 1B). The stimulus density defines an integer screen lattice. Each flow element is dropped onto this lattice, and then its position is perturbed by a normally distributed random variable. This destroys the impression of a perfectly regular grid of elements.

The displacement field is built on top of this and is organized around a screen partition consisting of a grid of rectangular or hexagonal tiles, with a single displacement vector within each tile. The tiles provide controllable flexibility in the motion. A planar translation results from choosing all displacement vectors the same. To avoid the impression of such simple translations, each displacement vector is “jittered” by sampling from a normal distribution, so that there are now both position jitter and motion jitter. More generally, one can develop more complex motions, either in geometry or in time, by varying the size of the tiles (discreteness) and by varying the displacement directions. For the experiments reported in this paper, a common mean and variance for all vectors in the field were used (see *SI Appendix, Materials and Methods* for specific parameter values).

The movement of each flow element is made even more “lifelike” by controlling its acceleration with a steering force computed as the difference between the element’s desired and current directions of motion. This behavior is based on the birds from ref. 46 and on the steering behavior described in ref. 47. Using this, the desired direction can be a function of both the underlying flow field and the proximity between elements; this guarantees that elements do not overlap one another, creating different geometries, densities, or sizes. The final force applied to each element is the resultant between the steering force and a repulsion force exerted by every other element within an allowed distance. The advantage of this approach is that the flow elements can make successive changes in direction as they drift through the flow field by following a smooth and continuous trajectory, without abrupt changes in direction or occlusion. They also wrap around the screen boundaries to preserve a constant number of patterns being shown at all times.

It remains to control the overall luminance and its changes, both for different stages in the trial and for the local dots. For some experiments, the screen luminance during the interstimulus period was set equal to the

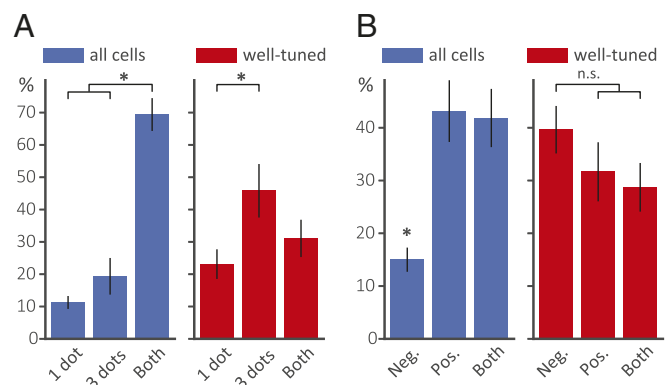


Fig. 5. Preference over flow stimuli variations. Percentages refer to the population of cells that had significant response to at least one flow variation. (A and B) All cells: $n = 667$, 10 experiments, six animals. Well-tuned cells: $n = 187$, 8 experiments, four animals. Error bars represent SEM (* $P < 0.001$). (A) Flow geometry preference. Among all cells responding significantly to flows, most showed no significant preference for either type. Among well-tuned cells, oriented flows were preferred over nonoriented flows. (B) Flow contrast polarity preference. Among all cells significantly responding to flows, positive polarity was preferred. The population of well-tuned cells showed no overall preference for contrast polarity. n.s., nonsignificant.

global average luminance of the stimulus used in the upcoming trial. This controls for responses that could be caused by the global change in the screen luminance only and not by the actual moving stimuli. However, for this strategy there will still be a change in the luminance of the background when the trial starts. To control for this, i.e., for possible responses due to changes in background luminance, we also ran experiments with a constant gray background both during the flow trials and during the inter-stimuli intervals. For dot-luminance effects, the diameter of each dot in a multidotted flow element was chosen such that the total area occupied by the element was the same as that of the single-dotted version of the

stimulus with the same spatial frequency. In any case, repeated experiments showed that there was little (if any) effect of these different luminance change variations. Code for generating the flow stimuli is available at <https://github.com/zuckerlab/FlowStims>.

ACKNOWLEDGMENTS. We are grateful to Dr. Sotiris Masmanides of University of California, Los Angeles for supplying the microelectrodes through the NSF NeuroNex program. This work was supported by the Simons Collaboration on the Global Brain, National Eye Institute Grant R01-EY02874, and National Science Foundation Grants CRCNS 1822650 and 1822598. M.P.S. is the recipient of the Research to Prevent Blindness Stein Innovation Award.

- Fenno L, Yizhar O, Deisseroth K (2011) The development and application of optogenetics. *Annu Rev Neurosci* 34:389–412.
- Niell CM, Stryker MP (2010) Modulation of visual responses by behavioral state in mouse visual cortex. *Neuron* 65:472–479.
- Fu Y, et al. (2014) A cortical circuit for gain control by behavioral state. *Cell* 156:1139–1152.
- Reimer J, et al. (2014) Pupil fluctuations track fast switching of cortical states during quiet wakefulness. *Neuron* 84:355–362.
- McGinley MJ, et al. (2015) Waking state: Rapid variations modulate neural and behavioral responses. *Neuron* 87:1143–1161.
- Hess EH, Polt JM (1960) Pupil size as related to interest value of visual stimuli. *Science* 132:349–350.
- Vinck M, Batista-Brito R, Knoblich U, Cardin JA (2015) Arousal and locomotion make distinct contributions to cortical activity patterns and visual encoding. *Neuron* 86:740–754.
- Prusky GT, West PW, Douglas RM (2000) Behavioral assessment of visual acuity in mice and rats. *Vision Res* 40:2201–2209.
- Harris KD, Thiele A (2011) Cortical state and attention. *Nat Rev Neurosci* 12:509–523.
- Carandini M, Churchland AK (2013) Probing perceptual decisions in rodents. *Nat Neurosci* 16:824–831.
- Hoy JL, Yavorska I, Wehr M, Niell CM (2016) Vision drives accurate approach behavior during prey capture in laboratory mice. *Curr Biol* 26:3046–3052.
- Niell CM, Stryker MP (2008) Highly selective receptive fields in mouse visual cortex. *J Neurosci* 28:7520–7536.
- Juavinett AL, Callaway EM (2015) Pattern and component motion responses in mouse visual cortical areas. *Curr Biol* 25:1759–1764.
- Palagina G, Meyer JF, Smirnakis SM (2017) Complex visual motion representation in mouse area V1. *J Neurosci* 37:164–183.
- Douglas R, Neve A, Quittenbaum J, Alam N, Prusky G (2006) Perception of visual motion coherence by rats and mice. *Vision Res* 46:2842–2847.
- Stirman JN, Townsend LB, Smith SL (2016) A touchscreen based global motion perception task for mice. *Vision Res* 127:74–83.
- Carandini M, et al. (2005) Do we know what the early visual system does? *J Neurosci* 25:10577–10597.
- Froudarakis E, et al. (2014) Population code in mouse V1 facilitates readout of natural scenes through increased sparseness. *Nat Neurosci* 17:851–857.
- Rikhye RV, Sur M (2015) Spatial correlations in natural scenes modulate response reliability in mouse visual cortex. *J Neurosci* 35:14661–14680.
- Ruderman DL, Bialek W (1994) Statistics of natural images: Scaling in the woods. *Phys Rev Lett* 73:814–817.
- Simoncelli EP, Olshausen BA (2001) Natural image statistics and neural representation. *Annu Rev Neurosci* 24:1193–1216.
- Zucker SW (1986) The fox and the forest: Toward a type I/type II constraint for early optical flow. *Proceedings of the ACM SIGGRAPH/SIGART Interdisciplinary Workshop on Motion: Representation and Perception*, eds Badler N, Tsotsos JT (Elsevier North-Holland, Amsterdam), pp 29–62.
- Abraham R, Marsden JE, Marsden JE (1978) *Foundations of Mechanics* (Benjamin/Cummings Publishing, Reading, MA), Vol 36.
- Glass L (1969) Moire effect from random dots. *Nature* 223:578–580.
- Link NK, Zucker SW (1987) Sensitivity to corners in flow patterns. *Spat Vision* 2:233–244.
- Zucker SW (1985) Early orientation selection: Tangent fields and the dimensionality of their support. *Comp Vision Graphics Image Process* 32:74–103.
- Hubel DH, Wiesel TN (1959) Receptive fields of single neurones in the cat's striate cortex. *J Physiol* 148:574–591.
- Fairhall A (2014) The receptive field is dead. Long live the receptive field? *Curr Opin Neurobiol* 25:ix–xii.
- Schwartz O, Pillow JW, Rust NC, Simoncelli EP (2006) Spike-triggered neural characterization. *J Vis* 6:484–507.
- Mante V, Sussillo D, Shenoy KV, Newsome WT (2013) Context-dependent computation by recurrent dynamics in prefrontal cortex. *Nature* 503:78–84.
- Eichenbaum H (2017) Barlow versus Hebb: When is it time to abandon the notion of feature detectors and adopt the cell assembly as the unit of cognition? *Neurosci Lett* 680:88–93.
- Iacarusso MF, Gasler IT, Hofer SB (2017) Synaptic organization of visual space in primary visual cortex. *Nature* 547:449–452.
- Yuste R (2015) From the neuron doctrine to neural networks. *Nat Rev Neurosci* 16:487–497.
- Krapp HG, Hengstenberg B, Hengstenberg R (1998) Dendritic structure and receptive-field organization of optic flow processing interneurons in the fly. *J Neurophysiol* 79:1902–1917.
- Anzai A, Peng X, Van Essen DC (2007) Neurons in monkey visual area v2 encode combinations of orientations. *Nat Neurosci* 10:1313–1321.
- Clark DA, et al. (2014) Flies and humans share a motion estimation strategy that exploits natural scene statistics. *Nat Neurosci* 17:296–303.
- Self MW, et al. (2014) Orientation-tuned surround suppression in mouse visual cortex. *J Neurosci* 34:9290–9304.
- Samonds JM, Feese BD, Lee TS, Kuhlman SJ (2017) Nonuniform surround suppression of visual responses in mouse V1. *J Neurophysiol* 118:3282–3292.
- Adesnik H, Bruns W, Taniguchi H, Huang ZJ, Scanziani M (2012) A neural circuit for spatial summation in visual cortex. *Nature* 490:226–231.
- Allman J, Miezin F, McGuinness E (1985) Stimulus specific responses from beyond the classical receptive field: Neurophysiological mechanisms for local-global comparisons in visual neurons. *Annu Rev Neurosci* 8:407–430.
- Knierim JJ, Van Essen DC (1992) Neuronal responses to static texture patterns in area V1 of the alert macaque monkey. *J Neurophysiol* 67:961–980.
- Zipser K, Lamme VA, Schiller PH (1996) Contextual modulation in primary visual cortex. *J Neurosci* 16:7376–7389.
- Ohki K, Reid RC (2007) Specificity and randomness in the visual cortex. *Curr Opin Neurobiol* 17:401–407.
- Ben-Shahar O, Zucker SW (2004) Geometrical computations explain projection patterns of long-range horizontal connections in visual cortex. *Neural Comput* 16:445–476.
- Dadarlat MC, Stryker MP (2017) Locomotion enhances neural encoding of visual stimuli in mouse V1. *J Neurosci* 37:3764–3775.
- Reynolds CW (1987) Flocks, herds and schools: A distributed behavioral model. *ACM Computer Graphics* 21:25–34.
- Reynolds CW (1999) Steering behaviors for autonomous characters. *Proceedings of the 1999 Game Developers Conference* (Miller-Freeman, San Francisco), pp 763–782.